a broad range of rotational barriers), it is interesting that by using only structural and dynamic data it can be deduced that in the transition state of the two-ring flip the two rings are nearly perpendicular to the C=C plane.[33]

Relationships between Dynamic, Equilibria, and Structural Parameters. The linear relationship between dynamic ($\Delta G^{\ddagger}_{c}$) and structural (α_4, ϕ_2, etc.) parameters is complementary to previously reported[14] linear correlation between the $\Delta G^{\ddagger}_{c}$ and the keto $\rightleftharpoons$ enol (ΔG°) equilibria[34] for the same enols.

Conclusions. Replacement of the vinyl hydrogen in **1** by an alkyl group results in a shift in the threshold rotational mechanism from a one-ring to a two-ring flip. The present work and the similar complementary behavior observed for trimesitylvinyl systems[4] suggest that when the double bond substituent is small the passage of the ring cis to it through the C=C plane becomes energetically feasible. Consequently there is a shift in threshold mechanism from (n)-aryl ring flip to ($n - 1$)-aryl ring flip. This is in contrast with Ar_3CX molecular propellers where the threshold mechanism was consistently the two-ring flip.[8]

(33) Note that if the transition-state conformation of the two-ring flip is chiral, it should exist in two enantiomeric forms. A similar calculation to that described above but using the enantiomeric conformations of **1–5** should result in an enantiomeric (if the transition state is chiral) or identical (if the transition state is achiral) conformation.

(34) The caption of the linear ΔG° vs $\Delta G^{\ddagger}_{c}$ plot displayed in Figure 2 of ref 14 is erroneously exchanged with that of Figure 3.

Experimental Section

Infrared spectra were taken with a Perkin-Elmer 157 G spectrometer. ^{1}H NMR spectra were recorded on a Bruker WP 200 SY and WH-300 pulsed FT spectrometer equipped with an Aspect 2000 computer. Temperature measurements were based on the chemical shift separation of the protons of a methanol sample and utilization of the temperature shift correlation of Van Geet.[35]

2,2-Dimesitylvinyl Isopropyl Ether (6). To a solution of 2,2-dimesitylethenol (120 mg, 0.4 mmol) and benzyltriethylammonium bromide (25 mg, 0.1 mmol) in 2-bromopropane (5 mL), a solution of 50% aqueous NaOH (5 mL) was added, and the mixture was stirred at room temperature overnight. Ether (20 mL) was then added, the phases separated, and the organic phase washed with water (2 × 10 mL), dried ($MgSO_4$), and evaporated. The residue was recrystallized from ethanol to give colorless crystals (80 mg, 67%) of **6**: mp 125–6 °C; ν_{max} (Nujol) 1650 cm^{-1}; MS, m/z 322 (M, 72%), 280 (B, $Mes_2C{=}CHOH^+$). Anal. Calcd for $C_{23}H_{30}O$: C, 85.66; H, 9.38. Found: C, 85.88; H, 9.54.

Acknowledgment. We are indebted to Dr. L. Radom for helpful discussions. This work was supported by a grant from the United States–Israel Binational Science Foundation (BSF) Jerusalem, to whom we are grateful.

Registry No. 1, 54288-04-9; **2**, 89959-15-9; **3**, 96040-90-3; **4**, 96040-91-4; **5**, 89959-16-0; **6**, 118071-22-0.

(35) Van Geet, A. L. *Anal. Chem.* **1968**, *40*, 2227; **1970**, *42*, 679.

Comparison of Classical Simulations of the H + H_2 Reaction to Accurate Quantum Mechanical State-to-State Partial Cross Sections with Total Angular Momenta J = 0–4 and to Experiment for All J

Meishan Zhao,[†] Mirjana Mladenovic,[†] Donald G. Truhlar,*[,†] David W. Schwenke,[‡] Yan Sun,[⊥] Donald J. Kouri,[⊥] and Normand C. Blais[∥]

Contribution from the Department of Chemistry, Chemical Physics Program, and Supercomputer Institute, University of Minnesota, Minneapolis, Minnesota 55455, Eloret Institute, Sunnyvale, California 94087, Department of Chemistry and Department of Physics, University of Houston, Houston, Texas 77204-5641, and Chemistry Division, Los Alamos National Laboratory, Los Alamos, New Mexico 87545. *Received May 31, 1988*

Abstract: Quantum mechanical calculations are reported for probabilities and partial cross sections for the reaction H + p-H_2 ($v = 0, j = 0, 2, E_{rel} = 1.1$ eV, $J = 0$–4) → o-H_2 ($v' = 0, 1$) + H, where v, j, and v' are initial vibrational, initial rotational, and final vibrational quantum numbers, respectively, E_{rel} is the initial relative translational energy, and J is the conserved total angular momentum quantum number. The calculations involve three arrangements and 468–780 coupled channels, and they are converged to 0.1–1%. The corresponding quantities are also calculated by the quasiclassical trajectory method, and comparing these results provides a detailed test of the trajectory method. For most final states, the trajectory results agree with the quantal ones within a factor of 1.5 to 2, and the trajectory value for the ($v' = 1$)/($v' = 0$) branching ratio is too high by a factor of 1.6. We also report trajectory results that are converged with respect to increasing J, and the converged value of the branching ratio is found to be 2.5 times larger than experiment.

1. Introduction

Classical dynamical simulations are of great usefulness and interest in all branches of chemical dynamics.[1-5] The calculated results are often reasonable; in very few cases, however, has it been possible to test the absolute accuracy of classical methods for molecular collisions. The exception concerns atom–diatom and diatom–diatom collisions in the gas phase, for which the classical simulations take the form of the quasiclassical trajectory (QCT) method with semiclassical state initialization and histogram binning or smooth sampling algorithms for final-state assignment.[6]

[†] University of Minnesota.
[‡] Eloret Institute. Mailing address: NASA Ames Research Center, Mail Stop 230-3, Moffett Field, CA 94036.
[⊥] University of Houston.
[∥] Los Alamos National Laboratory.

(1) Marcus, R. A. In *Energy Storage and Redistribution in Molecules*; Hinze, J., Ed.; Plenum: New York, 1983; p 573.
(2) Raff, L. M.; Thompson, D. L. In *Theory of Chemical Reaction Dynamics*; Baer, M., Ed.; CRC Press: Boca Raton, FL, 1985; Vol. 3, p 1.
(3) Truhlar, D. G.; Dagdigian, P. J. *Comments At. Mol. Phys.* **1986**, *17*, 335.
(4) McCammon, J. A. *Repts. Progr. Phys.* **1984**, *47*, 1.
(5) Hynes, J. T. *Annu. Rev. Phys. Chem.* **1985**, *36*, 573.

0002-7863/89/1511-0852$01.50/0

Extensive comparisons of classical and quantal dynamics are available for inelastic collisions[7-10] and collinear atom–diatom reactions.[2,11,12] The quantal calculations of Schatz and Kuppermann[13] for the three-dimensional H + H_2 reaction at low collision energies were compared[13-16] to quasiclassical trajectory calculations[14,16-19] for a very approximate semiempirical[20] potential energy surface. Accurate[21] and approximate[16,22-25] quantal calculations for H + H_2 and H + D_2 by Light, Schatz, and coworkers have been compared[23,25,26] to trajectory calculations[16,26-28] for a more accurate[29] surface. Recent advances in techniques for performing accurate quantal calculations of reactive scattering[30,31] have now made it possible for us to perform converged quantal calculations, including nonzero total angular momentum quantum number J, without dynamical approximations, for higher collision energies, and we have recently reported calculations for

$$H + p\text{-}H_2(v,j) \rightarrow o\text{-}H_2(v',j') + H \qquad (1)$$

(v and j denote vibrational and rotational quantum numbers, respectively) on an accurate potential energy surface at total energies above 1.4 eV with J up to 2.[32] In the present paper we present additional calculations and compare them to new trajectory calculations of the same quantities. Two of the previous comparisons[14,23] include vibrational–rotational product-state distributions, which are a special feature of the present study.

Interest in these comparisons is piqued by recent comparisons of trajectory results[28,33,34] and the quantal calculations mentioned above[32] to state-to-state experiments[35-37] for the H + D_2 and H + p-H_2 reactions, as well as the hope that such comparisons will soon be possible for the D + H_2 reaction.[38,39] There is a long history of testing approximate dynamical models for reaction 1, and we note that conclusions drawn in such studies often have widespread implications for the understanding of chemical reactivity in general.[40] Finally we note that the present paper involves a significant advance in our ability to solve the internuclear-motion Schrodinger equation for chemical reactions in that the largest calculations reported here involve 780 coupled channels whereas the largest such calculations we are aware of in a previously published paper or preprint is 513.[32]

2. Methods

2.1. Quantal Calculations. The methods for the quantal calculations are explained elsewhere. In particular the calculations were performed by the generalized Newton variational principle with rotationally coupled distortion potentials and an $\mathcal{L}^2$ basis set $\{\Phi_\beta\}_{\beta=1}^{N}$ for the expansion of the reactive amplitude density.[30,31] The basis functions are products of Arthurs–Dalgarno basis functions[41] for rotational and orbital degrees of freedom, a vibrational basis of isolated-diatomic eigenvectors $\chi_{\alpha v_j}$ in a harmonic primitive basis (where α denotes the arrangement, i.e., which atom is free, and v and j are diatomic vibrational and rotational quantum numbers, respectively), and distributed gaussians[42] for the radial translational basis.

The present quantal calculations were performed for the double many-body-expansion[43] (DMBE) potential energy surface. Calculations were performed for nine combinations of the conserved quantum numbers J and P where J is the total angular momentum and P is the parity. In addition to calculations reported previously for H + H_2[32] we performed calculations with $J = 3$ and 4 and up to 780 channels for the largest JP block.

The basic equation of the quantal calculations is

$$\mathbf{K} = \mathbf{K}^0 + \mathcal{K}^B + \mathbf{B}^T\mathbf{C}^{-1}\mathbf{B} \qquad (2)$$

where $\mathbf{K}$ is the full reactance matrix, $\mathbf{K}^0$ is the reactance matrix for the distortion potential, $\mathbf{K}^0 + \mathcal{K}^B$ is the distorted-wave Born approximation

$$B_{\beta n} = \langle \Phi_\beta | G^D \mathcal{U} | \psi^n \rangle \qquad (3)$$

$$C_{\beta\beta'} = \langle \Phi_\beta | G^D - G^D \mathcal{U} G^D | \Phi_{\beta'} \rangle \qquad (4)$$

G^D and ψ^n are respectively the Green's function and regular standing-wave solution (both block diagonal in αv) for the distortion potential, and $\mathcal{U}$ is the coupling potential, which couples the various αv subblocks, times $(-2\mu/\hbar^2)$ where μ is the generalized system reduced mass. From $\mathbf{K}$ we calculate the transition matrix $\mathbf{T}$, the absolute squares of whose elements are the completely resolved transition probabilities $P^{JP}_{\alpha vjl\alpha' v' j' l'}$, where α denotes the arrangement (1, 2, or 3, depending on which atom is free); v, j, and l denote initial vibrational, rotational, and orbital quantum numbers, respectively; and primes denote final values.

Reaction probabilities for given J, P, v, j, and l are of interest for testing convergence and are obtained from the completely resolved transition probabilities by summing, which yields

$$P^{JP}_{vjl} = \sum_{\alpha'=2}^{3} \sum_{v'} \sum_{j'} \sum_{l'} P^{JP}_{vjl\alpha' v' j' l'} \qquad (5)$$

State-to-state reaction probabilities $P^{J}_{vlv'j'}$ for a given total angular momentum are obtained by summing differently and averaging, which yields

(6) Truhlar, D. G.; Muckerman, J. T. In *Atom–Molecule Collision Theory*; Bernstein, R. B., Ed.; Plenum: New York, 1979; p 505.
(7) Duff, J. W.; Truhlar, D. G. *Chem. Phys.* **1975**, *9*, 243.
(8) Pattengill, M. In *Atom–Molecule Collision Theory*; Bernstein, R. B., Ed.; Plenum: New York, 1979; p 359.
(9) Truhlar, D. G.; Reid, B. P.; Zurawski, D. E.; Gray, J. C. *J. Phys. Chem.* **1981**, *85*, 786.
(10) Schwenke, D. W.; Truhlar, D. G.; Coltrin, M. E. *J. Chem. Phys.* **1987**, *87*, 983.
(11) Truhlar, D. G.; *J. Phys. Chem.* **1979**, *83*, 188.
(12) Lee, K. T.; Bowman, J. M.; Wagner, A. F.; Schatz, G. C. *J. Chem. Phys.* **1982**, *76*, 3563.
(13) Schatz, G. C.; Kuppermann, A. *J. Chem. Phys.* **1976**, *65*, 4668.
(14) Barg, G.-D.; Mayne, H. R.; Toennies, J. P. *J. Chem. Phys.* **1981**, *74*, 1017.
(15) Schatz, G. C. In *Potential Energy Surfaces and Dynamics Calculations*, Truhlar, D. G., Ed.; Plenum: New York, 1981; p 287.
(16) Schatz, G. C. *J. Chem. Phys.* **1983**, *79*, 5386.
(17) Karplus, M.; Porter, R. N.; Sharma, R. D. *J. Chem. Phys.* **1965**, *43*, 3259.
(18) Osherov, V. I.; Ushakov, V. G.; Lomakin, L. A. *Chem. Phys. Lett.* **1978**, *55*, 513.
(19) Mayne, H. R. *Chem. Phys. Lett.* **1979**, *66*, 487.
(20) Porter, R. N.; Karplus, M. *J. Chem. Phys.* **1964**, *40*, 1105.
(21) Walker, R. B.; Stechel, E. B.; Light, J. C. *J. Chem. Phys.* **1978**, *69*, 2922.
(22) Schatz, G. C. *Chem. Phys. Lett.* **1983**, *94*, 183.
(23) Schatz, G. C. *Chem. Phys. Lett.* **1984**, *108*, 532.
(24) Colton, M. C.; Schatz, G. C. *Chem. Phys. Lett.* **1986**, *124*, 256.
(25) Schatz, G. C. In *The Theory of Chemical Reaction Dynamics*; Clary, D. C., Ed.; D. *Reidel*: Dordrecht, 1986; p 1.
(26) Mayne, H. R.; Toennies, J. P. *J. Chem. Phys.* **1979**, *70*, 5314.
(27) Mayne, H. R.; Toennies, J. P. *J. Chem. Phys.* **1981**, *75*, 1794.
(28) Blais, N. C.; Truhlar, D. G. *Chem. Phys. Lett.* **1983**, *102*, 120.
(29) Truhlar, D. G.; Horowitz, C. J. *J. Chem. Phys.* **1978**, *68*, 2466. Erratum: *Ibid* **1979**, *71*, 1514.
(30) Schwenke, D. W.; Haug, K.; Truhlar, D. G.; Sun, Y.; Zhang, J. Z. H.; Kouri, D. J. *J. Phys. Chem.* **1987**, *91*, 6080.
(31) Schwenke, D. W.; Haug, K.; Zhao, M.; Truhlar, D. G.; Sun, Y.; Zhang, J. Z. H.; Kouri, D. J. *J. Phys. Chem.* **1988**, *92*, 3202.
(32) Mladenovic, M.; Zhao, M.; Truhlar, D. G.; Schwenke, D. W.; Sun, Y.; Kouri, D. J. *Chem. Phys. Lett.* **1988**, *146*, 358.
(33) Blais, N. C.; Truhlar, D. G.; Garrett, B. C. *J. Chem. Phys.* **1985**, *82*, 2300.
(34) Blais, N. C.; Truhlar, D. G. *J. Chem. Phys.* **1985**, *83*, 2201.
(35) Gerrity, D. P.; Valentini, J. J. *J. Chem. Phys.* **1979**, *79*, 5202; **1984**, *81*, 1298; **1985**, *82*, 1323; **1985**, *83*, 2207.
(36) Rettner, C. T.; Marinero, E. E.; Zare, R. N. In *Physics of Electronic and Atomic Collisions: Invited Papers from the XIIIth ICPEAC*; Eichler, J., Hertel, I. V., Stolterfoht, N., Eds.; North Holland: Amsterdam, 1985. Marinero, E. E.; Rettner, C. T.; Zare, R. N. *J. Chem. Phys.* **1984**, *80*, 4142.
(37) Nieh, J.-C.; Valentini, J. J. *Phys. Rev. Lett.* **1988**, *60*, 519.
(38) Blais, N. C.; Truhlar, D. G. *J. Chem. Phys.* **1988**, *88*, 5457.
(39) Buntin, S. A.; Giese, C. F.; Gentry, W. R. *J. Chem. Phys.* **1987**, *87*, 1443.
(40) Truhlar, D. G.; Wyatt, R. E. *Annu. Rev. Phys. Chem.* **1976**, *27*, 1.
(41) Arthurs, A. M.; Dalgarno, A. *Proc. R. Soc. London Ser. A* **1960**, *256*, 540.
(42) Hamilton, I. P.; Light, J. C. *J. Chem. Phys.* **1986**, *84*, 306.
(43) Varandas, A. J. C.; Brown, F. B.; Mead, C. A.; Truhlar, D. G.; Blais, N. C. *J. Chem. Phys.* **1987**, *86*, 6258.

$$P^{J}_{vjv'j'} = \frac{1}{2j+1} \sum_{\alpha' \neq \alpha} \sum_{P=+,-} \sum_{l} \sum_{l'} P^{JP}_{\alpha vjl\alpha' v'j'l'} \quad (6)$$

The state-to-state cross sections for a maximum value J_{max} of J are given by

$$\sigma_{vjv'j'}{}^{J_{max}}(E_{rel}) = \frac{\pi}{k_{vj}{}^2} \sum_{J=0}^{J_{max}} (2J+1) P^{J}_{vjv'j'}(E_{rel}) \quad (7)$$

where $\hbar k_{vj}$ is the initial relative momentum, and E_{rel} is the initial relative translational energy. The reaction cross section for a given final vibrational level is obtained by summing over j'.

$$\sigma_{vjv'}{}^{J_{max}}(E_{rel}) = \sum_{j'} \sigma_{vjv'j'}{}^{J_{max}}(E_{rel}) \quad (8)$$

The $(v'=1)/(v'=0)$ vibrational branching ratio for a given initial state is defined by

$$R_{vj}{}^{J_{max}}(E_{rel}) = \sigma_{vj1}{}^{J_{max}}(E_{rel}) / \sigma_{vj0}{}^{J_{max}}(E_{rel}) \quad (9)$$

Cross sections and vibrational branching ratios are the large J_{max} limits of the quantities in eq 7–9. (To facilitate comparison with the classical simulations, nuclear spin effects[44] were not included.) In the present paper we report accurate calculations of these quantities for $J_{max} = 4$. Except for J_{max}, the calculations are completely converged, as demonstrated by extensive convergence tests.

The calculations for a single JP block involve several steps.[31] First, the asymptotic diatomic Hamiltonian is diagonalized for each J in a harmonic oscillator basis of N(HO) functions. The integrals are calculated by Gauss–Hermite quadrature with N(HO) + 14 points. The ground-state wave function is used to generate optimized[45] quadrature nodes for later steps in the calculation.

Next, $\mathbf{K}^0$ and a multichannel distorted-wave half-integrated Green's function are calculated for each αv subblock by the finite difference boundary value method. This involves several parameters: N(F), the number of grid points; $R_{\alpha,1}$, the location of the first grid point; $R_{\alpha,N(F)}$, the location of the last grid point; $N^{QV}_{\alpha\alpha}$, the number of Gauss-ground-state quadrature nodes for single-arrangement vibrational integrals; and $N^{QA}_{\alpha\alpha}$, the number of Gauss–Legendre quadrature nodes for single-arrangement angular integrals.

The next step involves the calculation of the $\mathcal{H}^{\mathbf{B}}$, B, and C matrices, involving integrals over the half-integrated Green's functions, the coupling potential, the regular solutions for the distortion potential, and the basis functions. These integrations involve the parameters $N^{QV}_{\alpha\alpha}$ and $N^{QA}_{\alpha\alpha}$ for single-arrangement integrals again plus several additional parameters for the exchange integrals: $N^{QA}_{\alpha\alpha'}$, the number of Gauss–Legendre quadrature nodes for angular parts of exchange integrals; N^{QGL}, the number of Gauss–Legendre quadrature nodes in a single segment of integration over the radial translational coordinate R_α; N^{QS}, the number of such segments; and $R_{\alpha,max}$, the maximum value of R_α included in exchange integrals. Note that in the present calculations the exchange integrals over R_α are always started at $R_{\alpha,min} = R_{\alpha,1}$.

The next step consists of the calculation of $\mathbf{B}^T\mathbf{C}^{-1}\mathbf{B}$, which is carried out using the UDU^T Gaussian Elimination algorithm of LINPACK.[46] The order of the symmetric matrix $\mathbf{C}$ is

$$M = Nm$$

where N is the number of channels, and m is the number of distributed gaussian basis functions per channel. The gaussians were taken as equally spaced with centers at $R_\alpha = R_1{}^G, R_1{}^G + \Delta, R_1{}^G + 2\Delta, \ldots, R_m{}^G$. The width parameters for the gaussians were determined by fixing a value, typically 1.4, for the c parameter of Hamilton and Light.[42]

2.2. Quasiclassical Calculations. The methods used for the quasiclassical trajectory calculations are also presented elsewhere.[6,9,28,34,38,47] In particular we used the LSTH[29] potential energy surface and the correspondence rules $j_{classical} = (j + {}^1/_2)\hbar$ and $v_{classical} = (v + {}^1/_2)\hbar$ for selection of rotational and vibrational action variables, and we selected impact parameters b from classical $b\,db$ distributions with a maximum value b_{max} by a standard Monte Carlo method. This gives a distribution of classical total angular momenta $\vec{J}_{class}$. Final quantum numbers were assigned by the quadratic smooth sampling (QSS) method.[9,34]

In addition to presenting QCT results converged with respect to increasing b_{max} we also re-analyzed the QCT calculations with the specific goal of testing it for low values of total angular momentum. With the correspondence rule $J_{class} = (J + {}^1/_2)\hbar$, where $J_{class} = |\vec{J}_{class}|$, the border between trajectories corresponding more closely to $J = n$ and those corresponding more closely to $J = n + 1$, where n is an integer, occurs at $J_{class} = (n + 1)\hbar$. Therefore, to compare to quantal calculations with a finite, small J_{max}, we deleted all trajectories with $J_{class} > J_{max} + 1$ from the Monte Carlo ensemble and repeated the analysis. The resulting classical ensemble is labeled by J_{max}, rather than by the maximum value of J_{class}, for convenience in comparing to the quantal results.

2.3. Potential Energy Surfaces. Both potential energy surfaces used in this paper are believed to be accurate within a few tenths of a kcal/mol, and they agree well with each other.[29,43] Thus the differences in the surface representations are not expected to play any significant role in the comparison of the classical and quantal simulations. We have actually checked this by comparing classical simulations for both surfaces for 63 low-J partial cross sections for $D + H_2(v = 0, j = 1) \rightarrow HD(v', j') + H$. The results, converged to about 10% with repect to sampling statistics, agree within 1σ, 2σ, and 3σ (where σ is the standard deviation) in 79, 98, and 100%, respectively, of the cases.[48] This confirms that the differences in the surface representations do not affect our conclusions.

Table I. Channel Bases

	CB 1	CB 2	CB 3	CB 4
$j_{max}(v = 0)$	13	13	13	14
$j_{max}(v = 1)$	12	12	12	13
$j_{max}(v = 2)$	11	11	11	12
$j_{max}(v = 3)$	11	11	10	12
$j_{max}(v = 4)$	10	...	9	11
$N(JP = 3+)$	468	387	450	513
$N(JP = 4-)$	594	486	570	654

3. Results

All calculations in this paper are for a relative translational energy $E_{rel} = 1.1$ eV. This corresponds to a total energy $E = 1.369$ eV for the initial state $v = j = 0$ and to $E = 1.413$ eV for $v = 0$, $j = 2$.

3.1. Convergence Checks. Table I presents four sets of values of j_{max}, the maximum value of the rotational quantum number in a given αv block. Each set defines a channel basis (CB). The table also shows how many channels each CB yields for JP blocks 3+ and 4−. [Note: the parity P is the sign of $(-1)^{j+l}$.] Table II presents sets of numerical parameters for selected convergence checks for these parity blocks, and Tables III and IV present selected results from these runs.

First consider Table III. Most results are converged to 0.1% or better, although two of the completely resolved transition probabilities deviate from the others by about 1% when the $v = 4$ vibrational level is entirely omitted. The runs in Table III show excellent convergence with respect to location of the first and last gaussian, number of gaussians, gaussian width parameter, number of primitive harmonic oscillator functions, placement and spacings of the finite difference grid, orders of all quadratures, and integration limits of the exchange integrals. They also show excellent convergence with respect to $j_{max}(v = 3)$. Table III shows excellent convergence with respect to $j_{max}(v = 0, 1, 2)$ as well as with respect to the location of the last gaussian for $J = 4$. The results in Tables III and IV are only a subset of the many convergence runs we performed at both energies. For production runs (all four JP blocks at both energies), we used CB 1 and all other parameters had the same or similar values as those for run 3+/1; we used $m = 9$ for production at the higher energy and the more conservative $m = 10$ for the lower energy. The number of channels and open (i.e., energetic accessible) channels for CB 1 for each JP block and energy is given in Table V. In all cases all energetically accessible channels are included in the basis.

Another check on the convergence is provided by symmetry. Since symmetry is not assumed in calculating the solution, it provides a check. We found that transition probabilities to states with α' equals respectively 2 or 3 but otherwise identical, typically agree to six significant figures.

3.2. Partial and Total Cross Sections. Tables VI and VII compare the quasiclassical and quantal partial cross sections for the two different initial states represented significantly in the recent experiment of Nieh and Valentini[37] on reaction 1. First consider

(44) Truhlar, D. G. *J. Chem. Phys.* **1976**, *65*, 1008.
(45) Schwenke, D. W.; Truhlar, D. G. *Computer Phys. Commun.* **1984**, *34*, 57.
(46) Dongarra, J. J.; Moler, C. B.; Bunch, J. R.; Stewart, G. W. *LINPACK User's Guide*; Society for Industrial and Applied Mathematics: Philadelphia, 1979.
(47) Blais, N. C.; Truhlar, D. G. *J. Chem. Phys.* **1976**, *65*, 5335.
(48) Blais, N. C.; Truhlar, D. G., unpublished.

Table II. Parameters for Convergence Checks of Quantal Calculations at E = 1.369 eV

run[a]	3+/1[b]	3+/2	3+/7	3+/9	3+/10	4−/1	4−/2	4−/3
CB	1	1	1	2	3	1	1	4
N	468	468	468	387	450	594	594	654
m	10	11	9	9	9	10	9	10
$R_1^G(a_0)$[c]	2.047	1.880	2.047	2.047	2.047	2.047	2.047	2.047
$\Delta(a_0)$	0.335	0.335	0.335	0.335	0.335	0.335	0.335	0.335
$R_m^G(a_0)$	5.062	5.230	4.727	4.727	4.727	5.062	4.727	5.062
c	1.4	1.4	1.4	1.4	1.3	1.4	1.4	1.4
M	4680	5148	4212	3483	4050	5940	5346	6540
N(HO)	75	75	50	75	50	75	75	75
N(F)	524	524	845	524	560	524	524	524
$R_{\alpha,1}(a_0)$	0.336	0.336	0.336	0.336	0.429	0.336	0.336	0.336
$R_{\alpha,N(F)}(a_0)$	12.909	12.909	12.909	12.909	11.979	12.909	12.909	12.909
$N_{\alpha\alpha}^{QV}$	10	10	10	10	15	10	10	10
$N_{\alpha\alpha}^{QA}$	60	60	30	60	30	60	60	60
$N_{\alpha\alpha'}^{QA}$	60	60	50	60	50	60	60	60
N^{QGL}	12	12	14	12	12	12	12	12
N^{QS}	14	14	15	14	15	14	14	14
$R_>(a_0)$	5.30	5.30	6.24	5.30	5.30	5.30	5.30	5.30

[a] JP/run number. [b] J = 3, P = +, run number 1. [c] 1 a_0 = 0.5292 × 10^{-10} m.

Table III. Completely Resolved Transition Probabilities ($P^{JP}_{1vjl2v'j'l'}$) and Reaction Probabilities (P^{JP}_{vjl}) for J = 3, P = +, E = 1.369 eV

v	j	l	v'	j'	l'	3+/1[a]	3+/2	3+/7	3+/9	3+/10
0	1	3	0	1	3	0.028 73	0.028 72	0.028 75	0.028 66	0.028 75
			0	2	2	0.060 29	0.060 23	0.060 27	0.060 18	0.060 28
			0	2	4	0.013 00	0.013 00	0.013 00	0.012 97	0.013 00
			0	3	1	0.033 93	0.033 92	0.033 94	0.033 93	0.033 94
			0	3	3	0.029 35	0.029 34	0.029 35	0.029 35	0.029 36
			1	1	3	0.004 342	0.004 348	0.004 357	0.004 403	0.004 357
			1	3	1	0.001 419	0.001 418	0.001 419	0.001 426	0.001 418
			1	3	3	0.001 979	0.001 977	0.001 981	0.001 990	0.001 978
			1	3	5	0.000 281	0.000 281	0.000 283	0.000 282	0.000 282
			1	5	3	0.000 215	0.000 214	0.000 215	0.000 214	0.000 215
			1	5	5	0.001 283	0.001 278	0.001 283	0.001 282	0.001 284
			1	5	7	0.002 353	0.002 353	0.002 358	0.002 350	0.002 359
				total		0.546 3	0.546 1	0.546 4	0.546 0	0.546 5
0	2	2	1	1	3	0.006 309	0.006 318	0.006 324	0.006 368	0.006 319
			1	3	1	0.000 651	0.000 651	0.000 652	0.000 659	0.000 652
			1	3	3	0.002 074	0.002 071	0.002 075	0.002 086	0.002 075
			1	3	5	0.000 877	0.000 876	0.000 876	0.000 874	0.000 875
			1	5	3	0.001 489	0.001 487	0.001 490	0.001 486	0.001 492
			1	5	5	0.001 116	0.001 114	0.001 117	0.001 116	0.001 118
			1	5	7	0.001 158	0.001 158	0.001 158	0.001 155	0.001 158
				total		0.584 5	0.584 3	0.584 5	0.584 1	0.584 5
0	2	4	1	1	3	0.007 236	0.007 240	0.007 244	0.007 266	0.007 244
			1	3	1	0.004 386	0.004 384	0.004 386	0.004 380	0.004 382
			1	3	3	0.005 391	0.005 388	0.005 391	0.005 394	0.005 386
			1	3	5	0.000 653	0.000 654	0.000 654	0.000 655	0.000 654
			1	5	3	0.000 696	0.000 696	0.000 696	0.000 698	0.000 697
			1	5	5	0.001 086	0.001 085	0.001 086	0.001 082	0.001 087
			1	5	7	0.003 007	0.003 005	0.003 009	0.002 987	0.003 001
				total		0.760 7	0.760 6	0.760 7	0.760 8	0.760 7
0	3	1		total		0.535 8	0.535 7	0.535 8	0.535 9	0.535 8
0	3	3		total		0.602 3	0.602 4	0.602 3	0.602 5	0.602 3
0	3	5		total		0.717 7	0.717 9	0.717 6	0.718 0	0.717 6

[a] JP/run number.

Table VI for v = 0, j = 0. The QCT results agree with the quantal results within a factor of 1.5 to 2 for most final states for both J_{max} = 2 and J_{max} = 4. The QCT method underestimates most partial cross sections for the v' = 0 level and tends to overestimate the partial cross sections when v' = 1. A very significant aspect of the results is that the trends are about the same for both values of J_{max}. The agreement is reasonably encouraging since, although the relative translational energy is high, the quantum numbers are low, and very general considerations[6] indicate that low values of the quantum numbers provide the most severe test of classical methods. We next look to Table VII to see if raising the initial rotational quantum number from 0 (for which classical methods are especially suspect) to 2 improves the agreement. It does not, at least on the average, although the agreement for j = 2, J_{max} = 4 is better than for other cases. Nevertheless the trends in the comparison of trajectory results to quantum mechanics for both initial rotational states are quite similar.

3.3. Vibrational Branching Ratios. Table VIII summarizes the values for the vibrational branching ratio for all calculations for both initial rotational states as well as for the 298 K distribution (52% j = 0, 48% j = 2) of p-H_2 that corresponds to the experiment of Nieh and Valentini.[37] We show results for J_{max} = 2, based on three total-angular-momentum/parity blocks for j = 0 and five for j = 2, and results for J_{max} = 4, based on five and nine such blocks for the respective j states. The latter results involve the most summing and averaging over j', l', J, and l, and so they give the best estimate of how well quantum effects do or do not average out under such summing and averaging.

Table IV. Completely Resolved Transition Probabilities ($P^{JP}_{v_1j_1l_2v'j'l'}$) and Reaction Probabilities (P^{JP}_{vjl}) for $J = 4$, $P = -$, and $E = 1.369$ eV

v	j	l	v'	j'	l'	4−/1[a]	4−/2	4−/3
0	1	4	0	1	4	0.015 02	0.015 02	0.015 02
			0	2	3	0.051 19	0.051 17	0.051 19
			0	2	5	0.034 87	0.034 88	0.034 82
			0	3	2	0.005 47	0.055 46	0.055 47
			0	3	4	0.014 46	0.014 44	0.014 48
			0	3	6	0.002 537	0.002 536	0.002 536
			1	1	4	0.003 498	0.003 502	0.003 489
			1	2	3	0.004 766	0.004 767	0.004 762
			1	2	5	0.001 924	0.001 925	0.001 920
			1	3	2	0.002 429	0.002 429	0.002 430
			1	3	4	0.001 438	0.001 440	0.001 440
			1	3	6	0.000 210	0.000 209	0.000 210
			total			0.533 2	0.533 0	0.533 2
0	2	3	1	1	4	0.006 125	0.006 120	0.006 120
			1	2	3	0.007 403	0.007 406	0.007 394
			1	2	5	0.003 655	0.003 659	0.003 656
			1	3	2	0.002 306	0.002 301	0.002 304
			1	3	4	0.002 436	0.002 434	0.002 437
			1	3	6	0.000 380	0.000 379	0.000 381
			total			0.593 9	0.593 9	0.594 0
0	2	5	1	1	4	0.004 780	0.004 778	0.004 776
			1	2	3	0.008 104	0.008 107	0.008 108
			1	2	5	0.002 710	0.002 711	0.002 706
			1	3	2	0.006 003	0.005 996	0.006 009
			1	3	4	0.003 267	0.003 266	0.003 268
			1	3	6	0.000 384	0.000 384	0.000 385
			total			0.725 2	0.725 2	0.725 2
0	3	2	total			0.596 3	0.596 5	0.596 3
0	3	4	total			0.521 4	0.521 0	0.521 3

[a] JP/run number.

Table V. Number of Channels and Open Channels for Channel Basis 1

			open channels	
J	P	N	$E = 1.369$ eV	$E = 1.413$ eV
3	+	468	180	198
3	−	654	258	282
4	−	594	222	246
4	+	780	300	330

Table VI. Partial Cross Sections (Å^2) for the Reaction H + p-H_2 ($v = j = 0$) → o-H_2 ($v'j'$) + H at $E_{rel} = 1.1$ eV

v'	j'	QCT-QSS converged	QCT-QSS $J_{max} = 2$	QCT-QSS $J_{max} = 4$	quantal $J_{max} = 2$	quantal $J_{max} = 4$
0	1	0.052 (3)[a]	0.0093 (14)[a]	0.021 (2)	0.0132	0.0278
	3	0.106 (5)	0.0052 (10)	0.018 (2)	0.0038	0.0184
	5	0.148 (5)	0.0016 (5)	0.005 (1)	0.0031	0.0088
	7	0.159 (6)	0.0007 (3)	0.0013 (5)	0.0009	0.0029
	9	0.101 (5)	0.0003 (2)	0.0012 (5)	0.0003	0.0011
	11	0.014 (2)	[b]	[b]	[c]	[c]
	sum	0.580	0.0171	0.047	0.0214	0.0590
1	1	0.018 (2)	0.0030 (7)	0.008 (1)	0.0026	0.0062
	3	0.037 (3)	0.0010 (4)	0.0045 (9)	0.0006	0.0023
	5	0.032 (3)	0.0007 (3)	0.0021 (6)	0.0011	0.0030
	7	0.006 (1)	0.0005 (3)	0.0012 (4)	0.0001	0.0004
	9	0.0003 (2)	[b]	[b]	0	0
	11	[b]	0	0	0	0
	sum	0.093	0.0053	0.016	0.0044	0.0119
2	1	0.0021 (6)	0.0001 (1)	0.0003 (2)	0.0002	0.0003
	3	0.0009 (4)	0.0001 (1)	0.0001 (1)	[c]	[c]
	5	0.0004 (2)	[b]	[b]	0	0
	7	[b]	[b]	[b]	0	0
	sum	0.003	0.0002	0.0002	0.0002	0.0003

[a] One standard deviation in the last significant figure or figures, i.e., 0.052 ± 0.003 and 0.0093 ± 0.0014. [b] Less than 10^{-4}. [c] Less than 2×10^{-5}.

Table VII. Partial Cross Sections (Å^2) for the Reaction H + p-H_2 ($v = 0, j = 2$) → o-H_2 ($v'j'$) + H at $E_{rel} = 1.1$ eV

v'	j'	QCT-QSS converged	QCT-QSS $J_{max} = 2$	QCT-QSS $J_{max} = 4$	quantal $J_{max} = 2$	quantal $J_{max} = 4$
0	1	0.047 (3)	0.0050 (10)	0.015 (2)	0.0060	0.0160
	3	0.104 (5)	0.0062 (11)	0.019 (2)	0.0078	0.0244
	5	0.143 (6)	0.0022 (7)	0.010 (1)	0.0018	0.0097
	7	0.170 (6)	0.0007 (3)	0.0035 (8)	0.0011	0.0041
	9	0.124 (5)	0.0003 (2)	0.0007 (3)	0.0004	0.0014
	11	0.028 (2)	[a]	[a]	[b]	[b]
	sum	0.62 (1)	0.0146	0.048	0.0172	0.0557
1	1	0.023 (2)	0.0021 (6)	0.006 (1)	0.0026	0.0061
	3	0.031 (3)	0.0021 (7)	0.006 (1)	0.0011	0.0038
	5	0.036 (3)	0.0009 (4)	0.0025 (7)	0.0004	0.0013
	7	0.013 (2)	0.0004 (2)	0.0012 (5)	0.0002	0.0005
	9	0.0009 (4)	[b]	[b]	[b]	[b]
	11	[b]	0	0	0	0
	sum	0.10 (1)	0.0056	0.015	0.0041	0.0117
2	1	0.0024 (7)	0.0001 (1)	0.0005 (3)	0.0003	0.0010
	3	0.0014 (5)	[a]	0.0001 (1)	[b]	[b]
	5	0.0005 (3)	[a]	[a]	0	0
	7	[a]	[b]	[b]	0	0
	sum	0.004 (1)	0.0001	0.0006	0.0003	0.0010

[a] Less than 10^{-4}. [b] Less than 5×10^{-5}.

Table VIII. Vibrational Branching Ratios at $E_{rel} = 1.1$ eV

initial rot. state	method	J_{max}	$\sigma(v' = 1)/\sigma(v' = 0)$
$j = 0$	QCT-QSS	2	0.31
		4	0.34
		converged	0.15
	quantal	2	0.21
		4	0.20
$j = 2$	QCT-QSS	2	0.38
		4	0.31
		converged	0.17
	quantal	2	0.24
		4	0.21
52% $j = 0$, 48% $j = 2$	QCT-QSS	2	0.34
		4	0.33
		converged	0.16
	quantal	2	0.222
		4	0.206
	experiment	converged	0.064 ± 0.015

First we see that both trajectory calculations and quantum mechanics predict that the vibrational branching ratio is similar for the two initial states. Thus we discuss further only the results for the 298 K distribution. There are several noteworthy aspects of these results: Both theoretical methods predict similar branching ratios for $J_{max} = 2$ and $J_{max} = 4$, but the trajectory calculations predict that the ratio will eventually drop by about a factor of 2 from this low J_{max} plateau. This is very encouraging in a qualitative sense since the quantum mechanical plateau value is considerably greater than the experimental[37] value, which of course includes all J. However, the quantal result for $J_{max} = 4$ must decrease more than a factor of 2; the actual discrepancy with experiment is a factor of 3.2. This may be an indication that the trajectory calculation does not predict the J_{max} dependence of the branching ratio correctly.

The large errors in the classical predictions of the branching ratios for $J_{max} = 2$ and 4 in Table VIII lead us to be very cautious about the accuracy of classical mechanics even for predicting trends and ratios, and they imply to us that trajectory calculations provide only a very rough guide to vibrational energy disposal in this reaction.

3.4. Rotational Distributions. There is great interest in rotational distributions of the products of chemical reactions and in the predictive ability of trajectory calculations for such distributions.[34,49] We can use the present calculations to test trajectory

(49) Truhlar, D. G.; Dixon, D. A. In *Atom–Molecule Collision Theory*; Bernstein, R. B., Ed.; Plenum: New York, 1979; p 151.

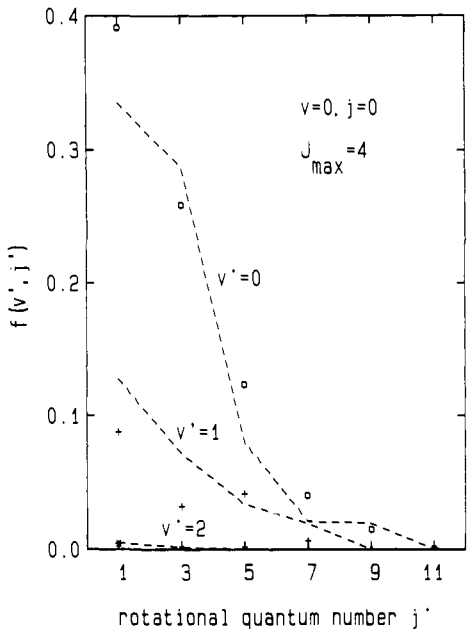

Figure 1. Fractional populations $f_{v=0,j=0}^{J_{max}=4}(v'j')$ as defined by eq 10. The quasiclassical results are shown as dashed lines. The quantal results are shown by circles for $v' = 0$, + for $v' = 1$, and * for $v' = 2$.

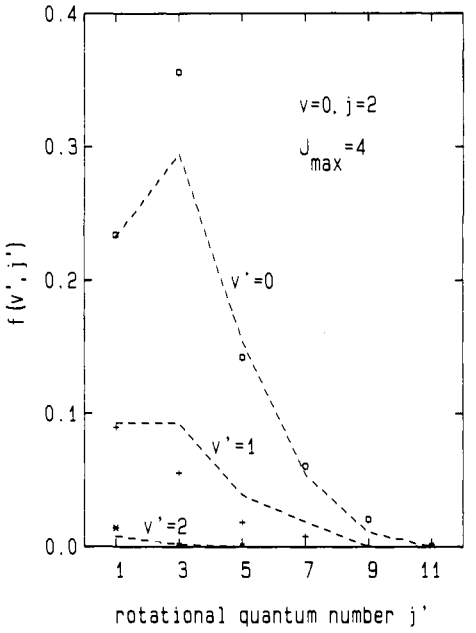

Figure 2. Same as Figure 1 except $v = 0, j = 2$.

calculations against converged quantum dynamics for these distributions. Thus we define the normalized product distributions by

$$f_{vj}^{J_{max}}(v'j') = \frac{\sigma_{vjv'j'}^{J_{max}}}{\sum_{v'}\sum_{j'}\sigma_{vjv'j'}^{J_{max}}} \quad (10)$$

These distributions are shown in Figures 1–4. Notice that j is even for the para reactant and odd for the ortho product.

Figures 1 and 2 present the quantal and the QCT–QSS distributions of eq 10 for $J_{max} = 4$; the QCT–QSS values converged with respect to J_{max} are shown in Figures 3 and 4. In all figures the initial state is indicated in the upper right corner, and the quasiclassical data are connected by straight lines to guide the eye. First look at Figures 1 and 2. Qualitatively, the quantal and the QCT–QSS distributions agree with one another quite well. In both calculations the most populated final state is $j' = 1$ when the initial state is $v = 0, j = 0$ (Figure 1). The rotationally excited

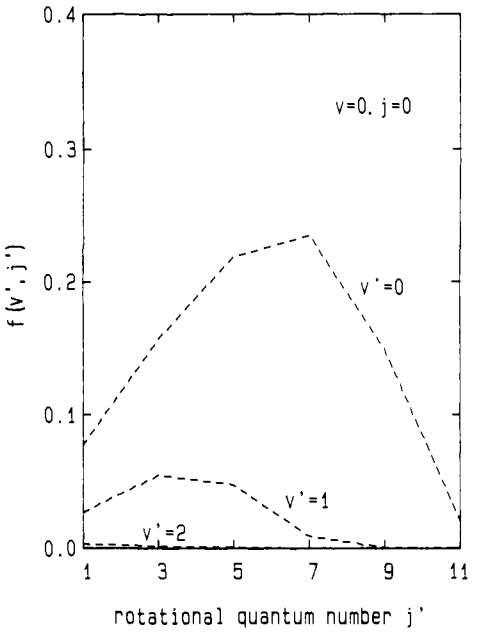

Figure 3. QCT–QSS values for $f_{v=0,j=0}^{J_{max}}(v'j')$ as defined by eq 10 and converged with respect to J_{max}.

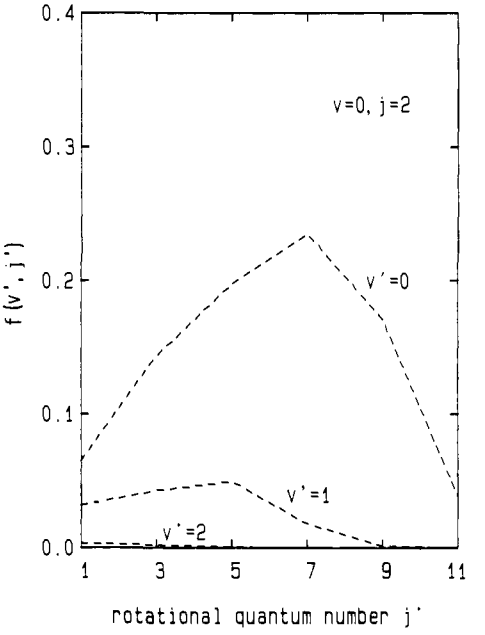

Figure 4. Same as Figure 3 except $v = 0, j = 2$.

reactant $v = 0, j = 2$ (Figure 2) shows the same behavior, in that the most probable j' is $j + 1$, only for the transitions to the ground final vibrational state; otherwise $j' = j - 1$ is most probable. The rotational distributions of products in the calculations that are converged with respect to J_{max} show a shift to higher j' quantum numbers, as can be seen in Figures 3 and 4. For both initial states the most populated final states are $j' = 7$ states if $v' = 0$. The first excited vibrational state $v' = 1$ of the products appears with greatest probability with $j' = j + 3$.

The partial reaction cross sections $\sigma^{J_{max}}(v' = 1, j' = 1, 3)$, thermally averaged over two initial rotational states at 298 K as for Table VIII, are given in Table IX. For transitions to $j' = 1$, the quantal and the QCT–QSS results agree quite well for both $J_{max} = 2$ and 4. The QCT–QSS result for $J_{max} = 4$ is a factor of 3 lower than the QCT–QSS value converged with respect to J_{max}, and the latter shows good agreement with the experimental result. The corresponding comparison for the transition into the more rotationally excited product state, $j' = 3$, shows a bigger difference between the quantal and the QCT–QSS results, i.e., for both $J_{max} = 2$ and 4 the quasiclassical result is bigger than

Table IX. Partial Cross Sections (Å^2) at E_{rel} = 1.1 eV, Thermally Averaged Over Initial Rotational States at 298 K

final rot. state	method	J_{max}	$\sigma(v' = 1,j')$
$j' = 1$	QCT–QSS	2	0.0026
		4	0.0070
		converged	0.020
	quantal	2	0.0026
		4	0.0062
	experiment	converged	0.019
$j' = 3$	QCT–QSS	2	0.0015
		4	0.0052
		converged	0.034
	quantal	2	0.00084
		4	0.0030
	experiment	converged	0.016

the quantal one by roughly a factor of 2. For this transiton, the J_{max} = 4 QCT–QSS result is 6.5 times smaller than the cross section converged with respect to J_{max}, while the latter is 2 times bigger than that experimentally obtained. Thus the QCT–QSS value converged with respect to J_{max} exceeds the experimental value by about the same ratio that the QCT–QSS J_{max} = 2 and 4 values exceed the quantal results. Therefore the fact that the trajectory calculations predict the $v' = 1, j' = 3$ state is produced with a cross section 1.7 times bigger than the $v' = 1, j' = 1$ state, while according to the experimental values the transition to $j' = 3$ is slightly less probable than that to $j' = 1$, may well be a consequence of the unreliability of the classical approach.

Examination of Tables VI and VII and Figures 1 and 2 shows very little structure, namely a local minimum for $v = j = 0$, $v' = 1, j' = 3$ and a local maximum for $v = 0, j = 2, v' = 0, j' = 3$. However, there is more structure if we look at reactive transitions into even j' states as well as odd ones (this is strictly for theoretical interpretative purposes, since when account is taken of atomic indistinguishability, the reactive transitions to even j' cannot be experimentally separated from the nonreactive ones). Figure 5 presents the state-to-state quantal cross sections for distinguishable-atom reactive collisions producing both even and odd j'. All results in these figures are for $v = 0$. As in Figures 1–4, the data are connected by straight lines and the state specification is indicated in the upper right corner. The curves in Figure 5 are for all five values of J_{max} (the highest curves correspond to J_{max} = 4). The results given in Figure 5 show three especially noteworthy features: (i) The two initial states produce similar rotational distributions for a specified final vibrational state v'. (ii) The shape of the distributions is strongly defined by v'. For the transitions into $v' = 0$, increasing the maximum total angular momentum from 0 to 4 moves the most probable j' value up by 1 and tends to destroy the structure for higher j'. (ii) For the transitions to $v' = 1$, the peak value of $\sigma(v' = 1, j')$ occurs at the same j' for all J_{max}, but higher j' states ($j' = 5$ for $j = 0$ and $j' = 6$ for $j = 2$) do become more pronounced as J_{max} increases.

3.5. Comparison to Previous Work. In ref 14, quasiclassical trajectory results[14] are compared to quantal ones[13] for $v = j = v' = 0$ and E_{rel} = 0.428 eV. The comparison is qualitatively similar to that for $v' = 0$ in Figure 1, i.e., the trajectory calculations are in semiquantitative agreement with quantum mechanics with the largest deviation at the peak value. At 0.428 eV, classical mechanics underestimates the peak in the normalized distribution at $j' = 1$ by about 35%; at 1.1 eV, where the deBroglie wavelengths in the various channels are smaller and many more quantum states are involved, with J_{max} = 4, classical mechanics underestimates this peak by about the same ratio. Thus high energy and the participation of many states, as well as summing over several total angular momenta, do not guarantee quantitative accuracy for rotational distributions.

The comparisons of ref 23 are particularly interesting because, although the quantal results in that study are approximate, the relative translational energy of 0.55 eV employed in that paper was the highest for which comparisons of reasonably accurate quantal results to trajectories were previously available. The approximate quantal calculations at 0.55 eV involved 17 JP blocks with up to 120 channels each; the final reaction cross section[23] was a factor of 1.6 higher than the result[28] calculated from quasiclassical trajectories. The present converged quantal calculations at 1.1 eV involve 9 JP blocks at each of two energies with up to 780 channels per block, and the final reaction cross sections are only 1.13 times higher than the quasiclassical values for $j = 0$ and 1.08 times higher for $j = 2$. The vibrational branching ratio is less than 2% at 0.55 eV, and this is too close to threshold for the quasiclassical results to be meaningful. At 1.1 eV, the quasiclassical vibrational branching ratio is still inaccurate by a factor of 1.6. The comparison of j' distributions for $v' = 0$ is more similar for the two energies although the agreement of trajectory results with quantal ones is better at the higher energy.

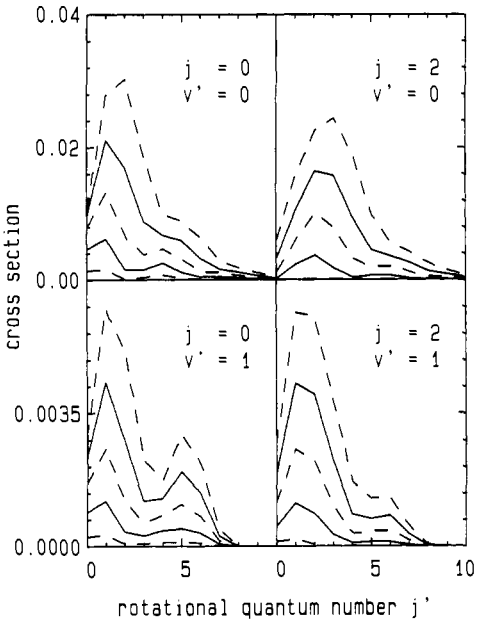

Figure 5. Quantal state-to-state cross sections in product levels $v' = 0$ and 1 from two initial states $v = 0, j = 0, 2$ as functions of the maximum total angular momentum J_{max} = 0, 1, 2, 3, 4. The J_{max} = 0 curve for $v = 0, j = 2, v' = 0$ can barely be seen since it is almost coincident with the abscissa on the scale shown.

4. Concluding Remarks

We have obtained converged solutions to the quantum mechanical equations describing a rearrangement collision with up to 780 coupled channels. The transition probabilities are converged to 0.1–1% or sometimes better. These results are used to test a quasiclassical trajectory calculation of partial cross sections for two values of the maximum angular momentum. The errors in the trajectory cross sections are a factor of 1.5 to 2.

The calculations also throw light on a recent comparison[32] of ab initio quantum dynamics with the experiment of Nieh and Valentini[37] for the product vibrational branching ratio in the H + p-$H_2 \rightarrow$ o-H_2 + H reaction. That comparison, in which the ab initio calculations are converged in all respects except that J_{max} = 2, showed two surprises: First, the experimental resonance features are stronger and narrower than the theoretical ones. Second, at high energy, e.g., a relative translational energy of 1.1 eV, the theoretical vibrational branching ratio $(v' = 1)/(v' = 0)$ is three times larger than experiment. The present calculations provide further data relevant to the second observation. First of all, extending the quantal calculations to J_{max} = 4 decreases the ab initio branching ratio only 7%. However, the quasiclassical trajectory calculations indicate that the vibrational branching ratio with converged J_{max} is a factor of 2 smaller than the quasiclassical J_{max} = 4 value and a factor of 1.3 smaller than the ab initio J_{max} = 4. This trend is very suggestive of a conclusion that the relative stability of the quantal vibrational branching ratios with respect to J_{max} over the ranges 0–2[32] and 2–4 (present results) are the consequence of low J_{max} plateau behavior rather than a more global

insensitivity of the vibrational branching ratios to angular momentum. Since the comparison summarized above shows that the quasiclassical results are not *quantitatively* reliable for this reaction, however, the remaining discrepancy between the quasiclassical result with converged J_{max} and the experiment must be resolved by further work. Although a quantal calculation with converged J_{max} will be difficult, the results should be very interesting when this calculation is available.

In summary, the main conclusions of this study are as follows. (1) Classical simulation of state-to-state chemical reaction probabilities for $H + p\text{-}H_2 \rightarrow o\text{-}H_2 + H$ are reliable to a factor of about 1.5, but not better. (2) Vibrational branching ratios for this reaction are relatively insensitive to total angular momentum for the range $0\text{-}4\hbar$ in both classical and quantal simulations, but the classical results are significantly lower at higher total angular momentum. (3) Classical simulations are in error by a factor of 2 for the final-state rotational partitioning into the two lowest rotational states of $o\text{-}H_2$ in the vibrationally excited level, even when contributions from two initial rotational states and nine total-angular-momentum/parity blocks are included. (4) Since the classical simulations are only semiquantitative at low angular momentum, further study of quantal effects at high angular momentum should prove very interesting.

Acknowledgment. This work was supported in part by the National Science Foundation, the R. A. Welch Foundation, and the Minnesota Supercomputer Institute.

Registry No. H, 12385-13-6; H_2, 1333-74-0.

Fragmentation and Structure of $C_2H_3S^+$ Ions

R. G. Cooks,*,† Md. A. Mabud,† S. R. Horning,† X.-Y. Jiang,† Cristina Paradisi,‡ and Pietro Traldi§

Contribution from the Department of Chemistry, Purdue University, West Lafayette, Indiana 47907, Dipartimento di Chimica Organica, Centro Meccanismi di Reazioni Organiche del CNR, Via Marzolo 1, 35131 Padova, Italy, and Area di Ricerca del CNR, Corso Stati Uniti 4, 35131 Padova, Italy. *Received October 7, 1987*

Abstract: Daughter spectra for $C_2H_3S^+$ ions, generated from a variety of precursor molecules and activated by different means, are insensitive to the nature of the precursors, but spectra recorded by different methods of activation show unexpectedly large differences. The methyl cation, a fragment characteristic of the thioacylium structure, is the dominant product of collisions at low energy with a gaseous or solid target but is virtually absent for zero scattering angle gas-phase collisions in the kiloelectronvolt range. As the scattering angle is increased, this low-energy fragment increases in abundance, and it is suggested that this is the result of an increased degree of direct vibrational as opposed to electronic excitation. It is shown that (i) the $C_2H_3S^+$ ions sampled by collision-activated dissociation and by surface-induced dissociation have the thioacylium structure, (ii) internal energy differences associated with their formation are not reflected in spectral changes in kiloelectronvolt collision experiments although they do affect the low-energy spectra, (iii) zero-angle, high-energy collisions probably involve fragmentation via excited electronic states, and for this reason they result in different products to those that occur upon low-energy collisions with gaseous or solid targets, and (iv) while activation by collision with a solid surface in the energy range below 100 eV causes very considerable internal excitation, only vibrational and not electronic excitation is involved. Isomerization between the several nascent $C_2H_3S^+$ structures generated from different precursors occurs prior to activation and is favored by the unusually high activation energy required for dissociation. When the highly endothermic charge stripping process is used, it is possible to sample some $C_2H_3S^+$ ions of such low internal energy that they have not completely isomerized.

The structure, energetics, and reactivity of gas-phase ions continues to generate wide interest.[1] Experimental strategies include analysis of gas-phase ion/molecule reactions,[2] which allows structural features to be inferred from the observed reactivity, and ion dissociation characteristics, best accomplished by means of tandem mass spectrometry (MS/MS).[3] The latter approach has gained wide popularity and has stimulated the development of new ion activation techniques. A typical experiment includes the following stages: (i) generation and mass selection of the ionic species of interest, (ii) activation to induce dissociation, and (iii) analysis of the resulting fragmentation products by comparison with the fragments produced by model ions of known structure.

Activation of mass-selected ions can be achieved in photodissociation experiments[4] and through collision with a stationary gas-phase target[5] in either the high-energy (kiloelectronvolt)[6] or low-energy (electronvolt)[7] range of laboratory ion kinetic energies. More recently, procedures have been developed for activation of ionic species through their interaction with a solid surface.[8] Of these methods, collision-activated dissociation (CAD), where activation is achieved through collision with neutral gas-phase targets, has been most widely used. Application of several different methods to a given problem has much to offer, particularly since the different methods can result in deposition of different amounts of internal energy into the ion.[9] In several recent studies of gas-phase ion structure, surface-induced dissociation has proved

† Purdue University.
‡ Centro Meccanismi di Reazioni Organiche del CNR.
§ Area di Ricerca del CNR.

(1) (a) Hehre, W. J.; Radom, L.; Schleyer, P. v. R.; Pople, J. A. *Ab Initio Molecular Orbital Theory*; Wiley: New York, 1986. (b) Holmes, J. L. *Org. Mass Spectrom.* **1985**, *2*, 169.
(2) Ausloos, P. J. *Interaction Between Ions and Molecules*; Plenum Press: New York, 1975.
(3) McLafferty, F. W., Ed. *Tandem Mass Spectrometry*; Wiley: New York, 1983.
(4) Bowers, M. T., Ed. *Gas Phase Ion Chemistry*; Academic Press: New York, 1984; Vol. 3.
(5) Cooks, R. G., Ed. *Collision Spectroscopy*; Plenum Press: New York, 1978.
(6) Todd, P. J.; McLafferty, F. W. In Reference 3, Chapter 7.
(7) Dawson, P. H.; Douglas, P. J. In Reference 3, Chapter 6.
(8) (a) Mabud, Md. A.; DeKrey, M. J.; Cooks, R. G. *Int. J. Mass Spectrom. Ion Procresses* **1985**, *65*, 285. (b) DeKrey, M. J.; Kenttämaa, H. I.; Wysocki, V. H.; Cooks, R. G. *Org. Mass Spectrom.* **1986**, *24*, 193. (c) DeKrey, M. J.; Mabud, Md. A.; Cooks, R. G.; Syka, J. E. P. *Int. J. Mass Spectrom. Ion Procresses* **1985**, *67*, 295. (d) Mabud, Md. A.; DeKrey, M. J.; Cooks, R. G.; Ast, T. *Int. J. Mass Spectrom. Ion Procresses* **1986**, *69*, 277. (e) Ast, T.; Mabud, Md. A.; Cooks, R. G. *Int. J. Mass Spectrom. Ion Procresses* **1988**, *82*, 131.
(9) Wysocki, V. H.; Kenttämaa, H. I.; Cooks, R. G. *Int. J. Mass Spectrom. Ion Procresses* **1987**, *75*, 181.

0002-7863/89/1511-0859$01.50/0